Journal of Materials Chemistry C

COMMUNICATION

View Article Online
View Journal | View Issue

Cite this: J. Mater. Chem. C, 2018, 6, 7734

Received 16th March 2018,
Accepted 4th June 2018

DOI: 10.1039/c8tc01285g

rsc.li/materials-c

Compositionally tunable ternary $Bi_2(Se_{1-x}Te_x)_3$ and $(Bi_{1-y}Sb_y)_2Te_3$ thin films *via* low pressure chemical vapour deposition†

Sophie L. Benjamin,[ab] C. H. (Kees) de Groot,[c] Chitra Gurnani,[ad] Samantha L. Hawken,[a] Andrew L. Hector,[a] Ruomeng Huang,*[c] Marek Jura,[e] William Levason,[a] Eleanor Reid,[a] Gillian Reid,*[a] Stephen P. Richards[a] and Gavin B. G. Stenning[e]

The inherently rapid ligand substitution kinetics associated with the novel and chemically compatible precursors, $[MCl_3(E^nBu_2)_3]$ (M = Sb, Bi; E = Se, Te), enable CVD growth of ternary $Bi_2(Se_{1-x}Te_x)_3$ and $(Bi_{1-y}Sb_y)_2Te_3$ thin films with very good compositional, structural and morphological control, for the first time. X-ray diffraction data follow Vegard's law and Raman bands shift linearly with the atom substitutions, indicating very well-distributed solid solutions.

Antimony and bismuth selenide and telluride, M_2E_3 (M = Sb, Bi; E = Se, Te), are layered narrow bandgap semiconductors; Bi_2Se_3 0.24 eV, Bi_2Te_3 0.16 eV and Sb_2Te_3 0.28 eV.[1,2] Their highly anisotropic hexagonal structures lead to a number of important properties. M_2E_3 are of particular interest as thermoelectric materials for near room temperature applications. n-Type Bi_2Te_3 and p-type Sb_2Te_3 may be used to produce thermoelectric generators if coupled electrically in series and thermally in parallel.[3–6] Thermoelectric materials typically require high electrical conductivities, whilst being thermally insulating. Electrical conductivities (σ) reported for the layered hexagonal M_2E_3 materials produced *via* a range of deposition methods are ~100–550 S cm^{-1} (Bi_2Se_3),[7] ~340–1780 S cm^{-1} (Bi_2Te_3)[8–12] and 104–1695 S cm^{-1} (Sb_2Te_3).[13–15] Sb_2Se_3, on the other hand, adopts an orthorhombic structure and with its comparatively larger band gap (1.1 eV), has intrinsically low electrical conductivity (10^{-6}–10^{-7} S cm^{-1}),[16] however, its high absorption coefficient (>10^5 cm^{-1})[17] and dielectric constant (29–18 within a 2 kHz to 2 MHz range)[18] are attractive for photovoltaics.[19,20] These materials are also important topological insulators[21,22] and candidates for spintronic devices.[14]

As a scalable and relatively inexpensive processing method, chemical vapour deposition (CVD) is very widely used for thin film deposition.[23] A number of CVD approaches have been employed for binary M_2E_3 film growth, most of which use multiple precursor sources, *e.g.* Bi_2Se_3: $BiMe_3$ + $SeEt_2/H_2$;[7] Bi_2Te_3: $BiMe_3$ + Te^iPr_2;[8] Sb_2Te_3: SbR_3 (R = Me, Et) + TeR_2 (R = Et, ^{i}Pr).[24,25] However, single source precursors (containing the metal and chalcogen within a single molecule) can offer advantages, including good control of the film stoichiometry, more efficient precursor use, and easier-to-handle precursors (less hydrolytically sensitive and less pyrophoric). A small number of single source precursors for CVD of binary M_2E_3 materials have been reported, including $[Bi\{(SePR_2)_2N\}_3]$ (R = Ph, ^{i}Pr),[26,27] whilst $[Sb\{(TeP^iPr_2)_2N\}_3]$[28] and $[Sb\{SeC_5H_3(Me\text{-}3)N\}_3]$[29] have been used to deposit Sb_2Te_3 and Sb_2Se_3, respectively, *via* aerosol assisted (AA)CVD. $[MeSb(E^nBu_2)_2]$ (E = Se, Te) produce Sb_2Se_3 and Sb_2Te_3 thin films *via* low pressure (LP)CVD.[13,30] We have used molecular complexes of early transition metal and main group chlorides, bearing neutral chalcogenoether ligands for LPCVD of binary metal chalcogenide thin films.[31–34] The possibility of selective deposition of oriented films onto defined regions of lithographically patterned substrates has also been realised using these types of precursors.[12] This selectivity could bring significant advantages in device fabrication, since, if the chalcogenide material can be deposited only onto pre-defined regions of patterned substrates, this would reduce the number of processing steps required (*e.g.* removing the need for back-etching), as well as reducing the volume of the chalcogenide material required.

Whilst commercial thermoelectric devices based upon n-type Bi_2Te_3 and p-type Sb_2Te_3 are available, significantly enhanced thermoelectric properties have been reported for ternary phases and superlattices of Bi_2Te_3 and Sb_2Te_3.[35,36] The ability to control the composition, morphology and crystallite sizes in thin films

[a] Chemistry, University of Southampton, Southampton SO17 1BJ, UK. E-mail: G.Reid@soton.ac.uk
[b] School of Science and Technology, Nottingham Trent University, Nottingham NG11 8NS, UK
[c] Electronics and Computer Science, University of Southampton, Southampton SO17 1BJ, UK. E-mail: R.Huang@soton.ac.uk
[d] School of Natural Sciences, Mahindra Ecole Centrale, Hyderabad, India
[e] ISIS Neutron and Muon Source, Rutherford Appleton Laboratory, Harwell Science and Innovation Campus, Didcot, OX11 0QX, UK

† Electronic supplementary information (ESI) available: Methods for the precursor syntheses and characterisation, LPCVD experiments and film characterisation, together with discussion of the binary M_2E_3 film characterisation and electrical properties. See DOI: 10.1039/c8tc01285g

of the related ternary materials is therefore of considerable interest to allow optimisation of their properties for various applications, most notably thermoelectrics and topological insulators.[37–41] For n-type Bi_2Te_3, this is best achieved by introducing Se, forming a solid solution of $Bi_2(Se_{1-x}Te_x)_3$. Optimisation of p-type Sb_2Te_3 can be achieved by incorporation of Bi, in $(Bi_{1-y}Sb_y)_2Te_3$. Previous work has mainly involved solid state or solution processing methods to produce the ternary materials, and usually as bulk materials rather than thin films.[35–41] CVD of thin films of these key ternary thin film materials with good compositional control, as well as structural/morphological control, would open up exciting application prospects. However, this is particularly challenging by conventional CVD methods involving multiple precursors.

We report here the new molecular precursors, $[BiCl_3(Se^nBu_2)_3]$, $[SbCl_3(Se^nBu_2)_3]$ and $[SbCl_3(Te^nBu_2)_3]$, demonstrate their utility as single source CVD precursors for binary Bi_2Se_3, Sb_2Se_3 and Sb_2Te_3 films, respectively, and, most significantly, we show that LPCVD using the appropriate combination of (chemically similar) precursors from this series, produces thin films of the two key ternary solid solutions, $Bi_2(Se_{1-x}Te_x)_3$ and $(Bi_{1-y}Sb_y)_2Te_3$ with very good compositional, structural and morphological control.

Precursors

Whilst a number of CVD reagents for Bi_2Se_3 thin film deposition are known (*vide supra*), the previously unknown analogues of the precursor we used to deposit Bi_2Te_3, *i.e.* $[BiCl_3(Te^nBu_2)_3]$, were prepared with the intention of achieving chemical compatibility between the precursor types. The target compounds, $[BiCl_3(Se^nBu_2)_3]$, $[SbCl_3(Se^nBu_2)_3]$ and $[SbCl_3(Te^nBu_2)_3]$, were obtained in good yield as illustrated in Scheme 1, and have been shown to be suitable for LPCVD of the respective binary M_2E_3 thin films, with compositional, structural and electrical properties indicative of high quality materials (ESI†).

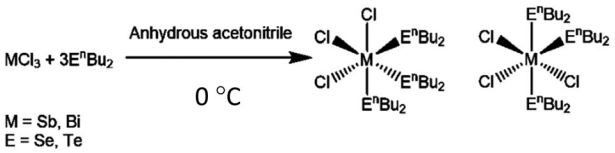

Scheme 1 Synthesis of the precursor complexes.

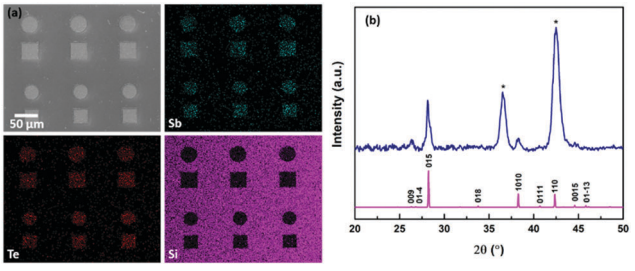

Fig. 1 (a) SEM image with EDX mapping and (b) grazing incidence XRD pattern from Sb_2Te_3 selectively deposited from $[SbCl_3(Te^nBu_2)_3]$ into 30 µm TiN holes and an indexed bulk pattern of Sb_2Te_3.[42] The TiN substrate peaks are marked by *.

We have shown previously that n-type Bi_2Te_3 can be selectively deposited into the TiN wells of lithographically patterned TiN/SiO_2 substrates using the precursor $[BiCl_3(Te^nBu_2)_3]$,[12] therefore, it was important to establish whether this could also be achieved for the p-type Sb_2Te_3. SEM images from depositions using ~15 mg of $[SbCl_3(Te^nBu_2)_3]$ at 723 K revealed that this is indeed the case (Fig. 1a). Quantitative EDX analysis revealed an Sb : Te ratio of 41% : 59% and grazing incidence XRD data are consistent with R-3mH Sb_2Te_3 (Fig. 1b).

LPCVD of ternary $Bi_2(Se_{1-x}Te_x)_3$ thin films

Our approach to deposit thin films of the ternary chalcogenide, $Bi_2(Se_{1-x}Te_x)_3$, exploits the inherent high lability of Bi(III) complexes with neutral donor ligands in solution. We have utilised the rapid ligand substitution kinetics of $[BiCl_3(E^nBu_2)_3]$ (E = Se, Te) to create mixed telluroether/selenoether complexes of $BiCl_3$ by combining various ratios of the precursors in CH_2Cl_2 solution prior to the CVD experiments. The relatively similar temperatures required for LPCVD of each of the binary M_2E_3 phases from this homologous pair of precursors was also promising for the LPCVD of the required $Bi_2(Se_{1-x}Te_x)_3$ ternary phase. At first sight, the need for a higher temperature for the Bi_2Se_3 deposition (550 °C) from $[BiCl_3(Se^nBu_2)_3]$ in comparison to that for LPCVD growth of Bi_2Te_3 (450 °C) was unexpected. However, this most likely reflects the presence of the weaker Te–C bonds in the latter (*cf.* the Se–C bonds in $[BiCl_3(Se^nBu_2)_3]$), arising from the orbital energy mismatch of the C and Te atoms. Hence, while the volatility of the higher MWt $[BiCl_3(Te^nBu_2)_3]$ precursor is expected to be lower than for the $[BiCl_3(Se^nBu_2)_3]$ precursor, this is offset by its lower thermal stability.

To test the hypothesis that these two precursors would be compatible for the optimisation of the target ternary $Bi_2(Se_{1-x}Te_x)_3$ phase by LPCVD, we initially studied the solution behaviour of $[BiCl_3(Te^nBu_2)_3]$ and $[BiCl_3(Se^nBu_2)_3]$, and mixtures thereof, by $^{77}Se\{^1H\}$ and $^{125}Te\{^1H\}$ NMR spectroscopy in CH_2Cl_2 solution (Fig. S7, ESI†). Each of solutions (i) to (iv) gave only one singlet at room temperature, indicating a rapidly exchanging mixture in solution. Introducing increasing amounts of $[BiCl_3(Te^nBu_2)_3]$ to a solution of $[BiCl_3(Se^nBu_2)_3]$ leads to a progressive shift of $\delta(^{77}Se)$ to lower frequency, while $\delta(^{125}Te)$ moves to higher frequency (*cf.* the individual parent complexes). Lowering the temperature to −80 °C causes only slight broadening of the resonances for each of the parent complexes (i) and (iv), and this was replicated for the mixed Se/Te samples ((ii) and (iii)). This behaviour is consistent with rapid ligand exchange (scrambling) in CH_2Cl_2 solution and the high lability of the $BiCl_3$ acceptor fragment, suggesting that the species present in solution are of the form $[BiCl_3\{(Se^nBu_2)_{1-m}(Te^nBu_2)_m\}_3]$ (m = 0 to 1) and hence this may be a possible reagent for LPCVD of the target ternary $Bi_2(Se_{1-x}Te_x)_3$ phase.

To test this hypothesis, a series of LPCVD experiments were undertaken by mixing different ratios of the two precursors to produce $[BiCl_3\{(Se^nBu_2)_{1-a}(Te^nBu_2)_a\}_3]$ with different values of a (from 0 to 3). Depositions were performed at 550 °C/0.05 mmHg

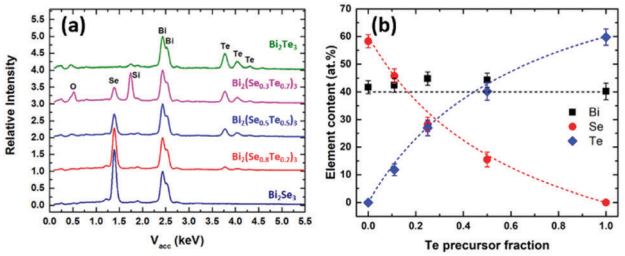

Fig. 2 (a) EDX spectra and (b) relationship between film composition and fraction of $[BiCl_3(Te^nBu_2)_3]$ used in the deposition of ternary $Bi_2(Se_{1-x}Te_x)_3$ films.

onto SiO_2-coated silicon substrates. In each case, reflective silvery films were obtained. EDX analyses (Fig. 2) revealed that the %Te content increases with increasing Te precursor amount, with a concomitant decrease in the %Se present. These data indicate very good control of the composition of the $Bi_2(Te_xSe_{1-x})_3$ ternary material using the $[BiCl_3(Te^nBu_2)_3]$/$[BiCl_3(Se^nBu_2)_3]$ precursor system. The %Te does not increase linearly with the fraction of the Te precursor used. Instead, it shows an enhancement in Te deposition. The enhancement factor can be calculated by the Te precursor fraction using eqn (1),

$$\%\mathrm{Te} = 0.6 \times \frac{m}{1 + (\alpha - 1)m} \quad (1)$$

where m is the Te precursor fraction and α is defined as the proposed 'enhancement factor'. The dotted lines in Fig. 2b represent the calculated %Te values using an enhancement factor, α of 2.5 and correspond well with the experimental values. This enhanced deposition of Te can be accounted for at least in part by the lower thermal stability of the $[BiCl_3(Te^nBu_2)_3]$ precursor due to the weaker Te–C bonds.

SEM (Fig. 3) analysis shows that the ternary films, like the binary parent materials, are polycrystalline, with good coverage across the substrate. In each case, film thicknesses of *ca.* 1 μm were obtained. The hexagonal crystallites are clearly visible, although their orientation varies; for the Bi_2Se_3 films, the crystallites appear to be aligned perpendicular to the substrate, whereas in the ternary and Bi_2Te_3 films most of the crystallites tend to lie parallel to the surface.

The phase purity and crystallinity of the as-deposited films were examined by grazing incidence XRD analysis (Fig. 4a).

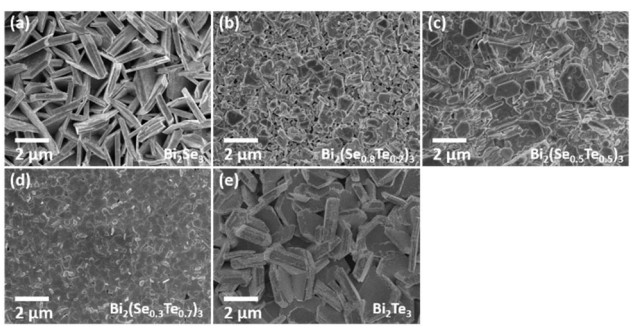

Fig. 3 SEM images showing the morphologies of the Bi_2Se_3 (a), Bi_2Te_3 (e) and ternary $Bi_2(Se_{1-x}Te_x)_3$ (b–d) films deposited by LPCVD under similar conditions (550 °C/0.05 mmHg) onto SiO_2-coated silicon substrates.

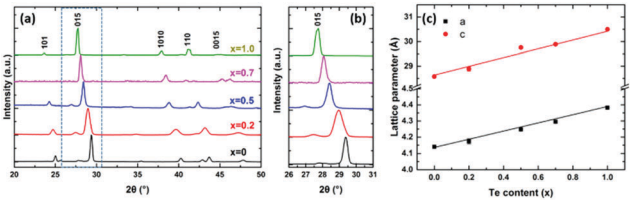

Fig. 4 (a) XRD patterns of as-deposited $Bi_2(Se_{1-x}Te_x)_3$ films with x ranging from 0 to 1; (b) expanded XRD patterns showing the systematic shift of the 015 peak; (c) refined lattice parameters (see Table S1, ESI†) as a function of the Te content for different as-deposited $Bi_2(Se_{1-x}Te_x)_3$ films.

All five films are isostructural, with no other phases detectable. A systematic shift of all the characteristic diffraction peaks with increasing Te composition is evident. Broadening of the 015 peak (Fig. 4b) for the $Bi_2(Se_{0.8}Te_{0.2})_3$, $Bi_2(Se_{0.5}Te_{0.5})_3$, $Bi_2(Se_{0.3}Te_{0.7})_3$ films can be observed, consistent with increased disorder in the structures due to Te doping. This disorder is also consistent with the decrease of the crystallite sizes for these three ternary compositions seen in Fig. 3. The lattice parameters (a, c) of all five compositions were refined against the Bi_2Se_3 phase from the ICSD.[43] Linear increases of both a and c with increasing Te content are observed (Fig. 4c), consistent with Vegard's law, *i.e.* well distributed solid solutions of the ternary $Bi_2(Se_{1-x}Te_x)_3$.

The vibrational properties of the as-deposited $Bi_2(Se_{1-x}Te_x)_3$ films were also studied by Raman spectroscopy. The spectra are shown in Fig. 5, where peaks are fitted using the Gaussian equation. For Bi_2Se_3 (Fig. 5a), two peaks positioned at 129 and 171 cm^{-1} can be assigned as E_g^2 (in-plane) and A_{1g}^2 (out-of-plane) modes, respectively, similar to previous reports.[44] These two vibrational modes are also present in the other four films, although they shift progressively to lower wavenumbers with increasing Te content (Fig. 5f). These results provide strong evidence for a very well-distributed solid solution.[38,39] An additional peak at *ca.* 120 cm^{-1} is detected for $Bi_2(Se_{0.3}Te_{0.7})_3$ and Bi_2Te_3 (Fig. 5d and e), ascribed to the A_{1u} mode, which is IR-active. The appearance of this peak implies the breaking of the crystal symmetry in the third dimension due to the limited thickness and the presence of the interfaces.[45,46]

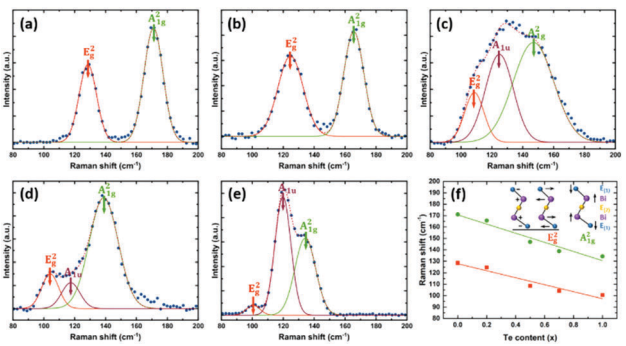

Fig. 5 (a–e) Raman spectra of as-deposited $Bi_2(Se_{1-x}Te_x)_3$ films with x ranging from 0 to 1. (f) Phonon frequencies (orange: E_g^2 mode; green: A_{1g}^2 mode) as a function of Te composition. The inset provides the schematic diagrams for the two Raman-active modes.

LPCVD of $(Bi_{1-y}Sb_y)_2Te_3$ thin films

To ascertain the compatibility of the precursors required for the target ternary $(Bi_{1-y}Sb_y)_2Te_3$ thin films, various ratios of $[MCl_3(Te^nBu_2)_3]$ (M = Bi and Sb) were analysed by $^{125}Te\{^1H\}$ NMR spectroscopy in CH_2Cl_2. In all cases, just one Te resonance was observed, consistent with the Te^nBu_2 ligands being labile and freely exchanging between the two weakly Lewis acidic MCl_3 units. A gradual change in chemical shift is observed with increasing Bi content, from 237 ppm for pure $[SbCl_3(Te^nBu_2)_3]$, to 262 ppm for pure $[BiCl_3(Te^nBu_2)_3]$.

In order to deposit the target ternary $(Bi_{1-y}Sb_y)_2Te_3$ films, different ratios of the $[BiCl_3(Te^nBu_2)_3]$ and $[SbCl_3(Te^nBu_2)_3]$ precursors were combined. In a typical LPCVD experiment, *ca.* 60 mg total mass of the reagents were combined in the chosen ratio, and the deposition was performed at 500 °C onto SiO_2 substrates, leading to silver-grey films across several substrates. Temperature profiling of the furnace revealed that when set to 500 °C, there was a temperature gradient from 270 °C at the edge of the furnace to 496 °C in the centre. Analysis of the films by XRD, EDX, SEM and Raman spectroscopy revealed that there was a variation in composition across the substrates, with increasing Sb content at higher deposition temperatures. The following analysis focuses on the films with the best coverage and showing a clear compositional variation with deposition temperature (across an 8 °C range from 474–482 °C), with the composition changing from Bi-rich at the cooler end, to Sb rich at the hotter end.

EDX analysis (Fig. 6a) was used to map the composition along the length of the sample (as a function of deposition temperature). Fig. 6b shows the change in %Sb content with temperature across the substrate; moving from lower to higher temperature the Bi content decreases. It also shows that the Sb-rich phases deposit within a very narrow temperature range. It is clear that Bi_2Te_3 deposits more easily at lower temperatures than Sb_2Te_3 and consequently, the Bi content in the vapour phase of the precursor is depleted in the early stages of the hot zone, which means it does not reach the substrates at higher temperatures.

SEM images (Fig. 7) taken at three positions (A–C) across the substrate show that the morphology is rather different from the regular hexagonal morphology observed for either Bi_2Te_3 or Sb_2Te_3. Moving along the substrate to the more Sb-rich phase, individual irregular-shaped plate-like crystallites are observed, rather than regular hexagons.

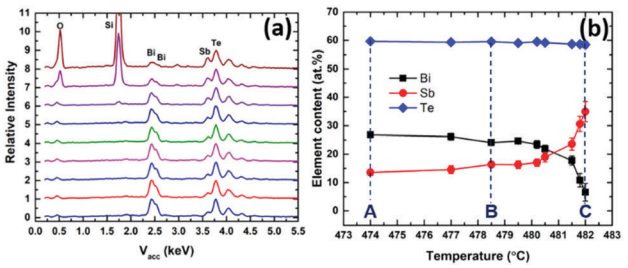

Fig. 6 (a) EDX spectra and (b) relationship between $(Bi_{1-y}Sb_y)_2Te_3$ film composition and the increasing temperature of deposition (indicating the temperatures at positions A, B and C).

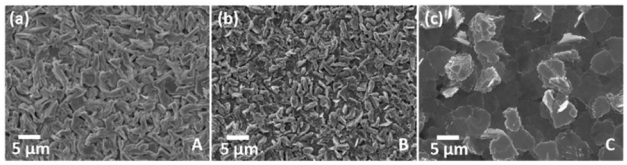

Fig. 7 SEM images of three regions (A–C) of the film deposited from a 1 : 1 ratio of $[SbCl_3(Te^nBu_2)_3]$ and $[BiCl_3(Te^nBu_2)_3]$ from Sb poor (a) to Sb rich (c).

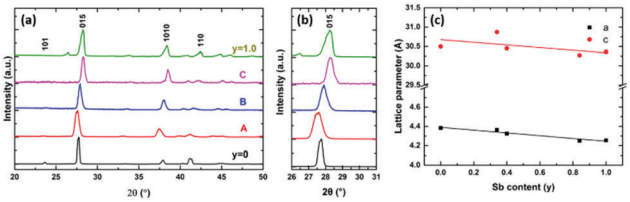

Fig. 8 (a) Grazing incidence XRD patterns from 3 positions (A–C; Sb poor to Sb rich) of a ternary sample deposited from a 1 : 1 ratio of $[SbCl_3(Te^nBu_2)_3]$ and $[BiCl_3(Te^nBu_2)_3]$, together with the binary phases (Sb_2Te_3 and Bi_2Te_3). Position A: a = 4.370(11) and c = 30.80(8) Å, position B: a = 4.327(8) and c = 30.54(8) Å, position C: a = 4.249(9) and c = 30.29(8) Å. (b) Expanded XRD patterns showing the systematic shift of the 015 peak; (c) refined lattice parameters as a function of the Sb content for different as-deposited $(Bi_{1-y}Sb_y)_2Te_3$ films.

Grazing incidence XRD data (Fig. 8) are consistent with a single phase (with no elemental Te) and show the reflections gradually shift from a lower 2θ value for Bi_2Te_3 to a higher 2θ value with increasing Sb content, as expected. The variation in the lattice parameters with Sb content is shown in Fig. 8c. Whilst the lattice parameter change is smaller in this system, there is an approximately linear trend, consistent with Vegard behaviour.

The composition of the film was also mapped with Raman spectroscopy (Fig. 9). This shows the shift in peaks from Bi_2Te_3 to Sb_2Te_3. The E_g^2 vibrational mode shifts from 100 to 120 cm^{-1} and the E_{1g}^2 mode shifts from 134 to 167 cm^{-1} showing the

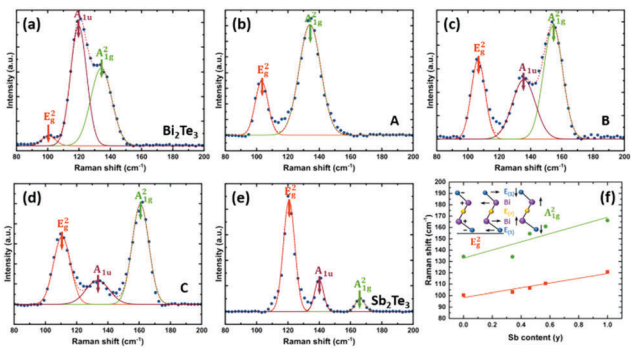

Fig. 9 (a–e) Raman spectra from 3 positions (Sb poor to Sb rich) of a ternary $(Bi_{1-y}Sb_y)_2Te_3$ sample deposited from a 1 : 1 ratio of $[SbCl_3(Te^nBu_2)_3]$ and $[BiCl_3(Te^nBu_2)_3]$, together with the binary phases (Sb_2Te_3 and Bi_2Te_3); (f) phonon frequencies (orange: E_g^2 mode; green: A_{1g}^2 mode) as a function of Sb composition. The inset provides the schematic diagrams for the two Raman-active modes.

change in composition of the solid solution of the ternary phase. This is consistent with Raman spectra of $(Bi_{1-y}Sb_y)_2Te_3$ deposited by solvothermal synthesis[47] and MBE.[37]

Conclusions

This work presents a chemically compatible library of molecular precursors suitable for the LPCVD growth of high quality binary M_2E_3 (M = Sb, Bi; E = Se, Te) thin films on silica. Moreover, their suitability to be combined in different ratios, producing rapidly scrambling precursor systems, allows a highly innovative route for the LPCVD of the key ternary $Bi_2(Se_{1-x}Te_x)_3$ and $(Bi_{1-y}Sb_y)_2Te_3$ films with very good compositional, structural and morphological control, as well-distributed solid solutions (following Vegard behaviour). In the case of $Bi_2(Se_{1-x}Te_x)_3$, the ternary composition is mainly governed by the relative ratios of the precursors used, whilst for $(Bi_{1-y}Sb_y)_2Te_3$, the deposition temperature has a greater influence on the film composition.

Good compositional, structural and morphological control across the ternary phase is very important for tuning the functional properties of the V–VI materials for applications in thermoelectric devices or topological insulators. This, coupled with the demonstration that our precursor system allows selective film growth onto defined regions of lithographically patterned substrates, suggests that using these new precursors in a CVD based approach offers exciting prospects for the fabrication of thin film micro-thermoelectric generators. This will form the basis of our future work.

Conflicts of interest

There are no conflicts to declare.

Acknowledgements

We thank the STFC for funding (ST/L003376/1 and ST/P00007X/1) and the EPSRC for a Case Award to S. L. H. (EP/M50662X/1). We also gratefully acknowledge funding for thin film diffraction and NMR instrumentation from the EPSRC through EP/K00509X, EP/K009877/1 and EP/K039466/1. C. G. thanks the Royal Society (London) for a Newton International Alumnus Award.

Notes and references

1 O. Madelung, *Semiconductors: Data Handbook*, Springer Berlin Heidelberg, Berlin Heidelberg, 2004, vol. 14.
2 T. C. Harman, B. Paris, S. E. Miller and H. L. Goering, *J. Phys. Chem. Solids*, 1957, **2**, 181–190.
3 G. J. Snyder and E. S. Toberer, *Nat. Mater.*, 2008, **7**, 105–114.
4 L. E. Bell, *Science*, 2008, **321**, 1457–1461.
5 V. A. Kutasov, L. N. Lukyanova and M. V. Vedernikov, in *Thermoelectrics Handbook: Macro to Nano*, ed. R. D. Michael, CRC Press, 2006, ch. 37.
6 C. J. Vineis, A. Shakouri, A. Majumdar and M. G. Kanatzidis, *Adv. Mater.*, 2010, **22**, 3970–3980.
7 A. Al Bayaz, A. Giani, A. Foucaran, F. Pascal-Delannoy and A. Boyer, *Thin Solid Films*, 2003, **441**, 1–5.
8 H. You, S. H. Baek, K.-C. Kim, O.-J. Kwon, J.-S. Kim and C. Park, *J. Cryst. Growth*, 2012, **346**, 17–21.
9 A. Akrap, A. Ubaldini, E. Giannini and L. Forro, *EPL*, 2014, **107**, 57008.
10 M. M. Rashid, K. H. Cho and G.-S. Chung, *Appl. Surf. Sci.*, 2013, **279**, 23–30.
11 N. Peranio, M. Winkler, Z. Aabdin, J. König, H. Böttner and O. Eibl, *Phys. Status Solidi A*, 2012, **209**, 289–293.
12 S. L. Benjamin, C. H. de Groot, C. Gurnani, A. L. Hector, R. Huang, E. Koukharenko, W. Levason and G. Reid, *J. Mater. Chem. A*, 2014, **2**, 4865–4869.
13 S. L. Benjamin, C. H. de Groot, A. L. Hector, R. Huang, E. Koukharenko, W. Levason and G. Reid, *J. Mater. Chem. C*, 2015, **3**, 423–430.
14 S. Zastrow, J. Gooth, T. Boehnert, S. Heiderich, W. Toellner, S. Heimann, S. Schulz and K. Nielsch, *Semicond. Sci. Technol.*, 2013, **28**, 035010 (6 pages).
15 P. Fan, Z. H. Zheng, G. X. Liang, D. P. Zhang and X. M. Cai, *J. Alloys Compd.*, 2010, **505**, 278–280.
16 L. R. Gilbert, B. Van Pelt and C. Wood, *J. Phys. Chem. Solids*, 1974, **35**, 1629–1632.
17 Y. Zhou, M. Leng, Z. Xia, J. Zhong, H. Song, X. Liu, B. Yang, J. Zhang, J. Chen, K. Zhou, J. Han, Y. Cheng and J. Tang, *Adv. Energy Mater.*, 2014, **4**, 1301846.
18 C. Chen, D. C. Bobela, Y. Yang, S. Lu, K. Zeng, C. Ge, B. Yang, L. Gao, Y. Zhao, M. C. Beard and J. Tang, *Front. Optoelectron.*, 2017, **10**, 18–30.
19 Y. C. Choi, T. N. Mandal, W. S. Yang, Y. H. Lee, S. H. Im, J. H. Noh and S. Il Seok, *Angew. Chem., Int. Ed.*, 2014, **53**, 1329–1333.
20 X. Liu, J. Chen, M. Luo, M. Leng, Z. Xia, Y. Zhou, S. Qin, D. J. Xue, L. Lv, H. Huang, D. Niu and J. Tang, *ACS Appl. Mater. Interfaces*, 2014, **6**, 10687–10695.
21 H. Zhang, C.-X. Liu, X.-L. Qi, X. Dai, Z. Fang and S. C. Zhang, *Nat. Phys.*, 2009, **5**, 438–442.
22 Y. Guo, Z. Liu and H. Peng, *Small*, 2015, **11**, 3290–3305.
23 A. C. Jones and M. L. Hitchman, in *Chemical Vapour Deposition: Precursors*, ed. A. C. Jones and M. L. Hitchman, The Royal Society of Chemistry, 2009, pp. 1–36.
24 A. Giani, A. Boulouz, F. P. Delannoy, A. Foucaran, A. Boyer, B. Aboulfarah and A. Mzerd, *J. Mater. Sci. Lett.*, 1999, **18**, 541–543.
25 J. H. Kim, Y. C. Jung, S. H. Suh and J. S. Kim, *J. Nanosci. Nanotechnol.*, 2006, **6**, 3325–3328.
26 J. Waters, D. Crouch, J. Raftery and P. O'Brien, *Chem. Mater.*, 2004, **16**, 3289–3298.
27 J. Waters, D. Crouch, P. O'Brien and J. H. Park, *J. Mater. Sci.: Mater.*, 2003, **4**, 599–602.
28 S. S. Garje, D. J. Eisler, J. S. Ritch, M. Afzaal, P. O'Brien and T. Chivers, *J. Am. Chem. Soc.*, 2006, **128**, 3120–3121.
29 R. K. Sharma, G. Kedarnath, V. K. Jain, A. Wadawale, M. Nalliath, C. G. S. Pillai and B. Vishwanadh, *Dalton Trans.*, 2010, **39**, 8779–8787.
30 R. Huang, S. L. Benjamin, C. Gurnani, Y. Wang, A. L. Hector, W. Levason, G. Reid and C. H. de Groot, *Sci. Rep.*, 2016, **6**, 27593 (10 pages).

31 S. D. Reid, A. L. Hector, W. Levason, G. Reid, B. J. Waller and M. Webster, *Dalton Trans.*, 2007, 4769–4777.
32 C. H. de Groot, C. Gurnani, A. L. Hector, R. Huang, M. Jura, W. Levason and G. Reid, *Chem. Mater.*, 2012, **24**, 4442–4449.
33 K. George, C. H. de Groot, C. Gurnani, A. L. Hector, R. Huang, M. Jura, W. Levason and G. Reid, *Chem. Mater.*, 2013, **25**, 1829–1836.
34 S. L. Benjamin, C. H. de Groot, C. Gurnani, A. L. Hector, R. Huang, K. Ignatyev, W. Levason, S. J. Pearce, F. Thomas and G. Reid, *Chem. Mater.*, 2013, **25**, 4719–4724.
35 R. Venkatasubramanian, E. Siivola, T. Colpitts and B. O'Quinn, *Nature*, 2001, **413**, 597–602.
36 X. Guo, X. Jia, K. Jie, H. Sun, Y. Zhang, B. Sun and H. Ma, *CrystEngComm*, 2013, **15**, 7236–7242.
37 C. Weyrich, M. Drögeler, J. Kampmeier, M. Eschbach, G. Mussler, T. Merzenich, T. Stoica, I. E. Batov, J. Schubert, L. Plucinski, B. Beschoton, C. M. Schneider, C. Stampfer, D. Grüzmacher and T. Tchäpers, *J. Phys.: Condens. Matter*, 2016, **28**, 495501.
38 M. Hong, T. C. Chasapis, Z.-G. Chen, L. Yang, M. G. Kanatzidis, J. Snyder and J. Zou, *ACS Nano*, 2016, **10**, 4719–4727.
39 A. Soni, Z. Yanyuan, Y. Ligen, M. K. K. Aik, M. S. Dresselhaus and Q. Ziong, *Nano Lett.*, 2012, **12**, 1203–1209.
40 J.-L. Mi, P. Norby, M. Bremholm and B. B. Iversen, *Chem. Mater.*, 2017, **29**, 5070–5079.
41 B. Xu, T. Feng, M.-T. Agne, L. Zhou, X. Ruan, G. J. Snyder and Y. Wu, *Angew. Chem., Int. Ed.*, 2017, **56**, 3546–3551.
42 T. L. Anderson and H. B. Krause, *Acta Crystallogr.*, 1974, **B30**, 1307–1310.
43 ICSD: Inorganic Crystal Structure Database (ICSD), Fachinformationszentrum Karlsruhe (FIZ), accessed *via* the EPSRC National Chemical Database Service hosted by the Royal Society of Chemistry.
44 (*a*) A. J. Barton, N. J. Hill, W. Levason, B. Patel and G. Reid, *Chem. Commun.*, 2001, 95–96; (*b*) A. J. Barton, N. J. Hill, W. Levason and G. Reid, *J. Chem. Soc., Dalton Trans.*, 2001, 1621–1627.
45 D. Teweldebrhan, V. Goyal and A. A. Balandin, *Nano Lett.*, 2010, **10**, 1209–1218.
46 K. M. F. Shahil, M. Z. Hossain, D. Teweldebrhan and A. A. Balandin, *Appl. Phys. Lett.*, 2010, **96**, 153103.
47 C. Zhang, Z. Peng, Z. Li, L. Yu, K. A. Khor and Q. Xiong, *Nano Energy*, 2015, **15**, 688–696.